



Walter+Eliza Hall  
Institute of Medical Research

## Research Publication Repository

<http://publications.wehi.edu.au/search/SearchPublications>

This is the author's version of the accepted article:	Vasanthakumar A, Xu D, Lun AT, Kueh AJ, van Gisbergen KP, Iannarella N, Li X, Yu L, Wang D, Williams BR, Lee SC, Majewski IJ, Godfrey DI, Smyth GK, Alexander WS, Herold MJ, Kallies A, Nutt SL, Allan RS. A non-canonical function of Ezh2 preserves immune homeostasis. <i>EMBO Reports</i> . 2017 18(4):619-631.
Final published version:	doi: 10.15252/embr.201643237
Terms of use:	Copyright© 2017 EMBO

## **A non-canonical function of Ezh2 in the preserves immune homeostasis**

Ajithkumar Vasanthakumar<sup>1,2\*</sup>, Dakang Xu<sup>6,7\*</sup>, Aaron Lun<sup>1,2</sup>, Andrew J. Kueh<sup>1,2</sup>, Klaas P.J.M. van Gisbergen<sup>1,2</sup>, Nadia Iannarella<sup>1</sup>, Xiaofang Li<sup>6,7</sup>, Liang Yu<sup>7</sup>, Die Wang<sup>7</sup>, Bryan R.G. Williams<sup>7</sup>, Stanley C. W. Lee<sup>1,2</sup>, Ian J. Majewski<sup>1,2</sup>, Dale I. Godfrey<sup>4,5</sup>, Gordon K. Smyth<sup>1,3</sup>, Warren S. Alexander<sup>1,2</sup>, Marco J. Herold<sup>1,2</sup>, Axel Kallies<sup>1,2</sup>, Stephen L. Nutt<sup>1,2#</sup> & Rhys S. Allan<sup>1,2#</sup>

<sup>1</sup>The Walter and Eliza Hall Institute of Medical Research, Parkville, Victoria, 3052, Australia.

<sup>2</sup>Department of Medical Biology, <sup>3</sup>Department of Mathematics and Statistics, <sup>4</sup>Department of Microbiology and Immunology, <sup>5</sup>ARC Centre of Excellence for Advanced Molecular Imaging, The University of Melbourne, Parkville, Victoria, 3010, Australia.

<sup>6</sup>Institute of Ageing Research, Hangzhou Normal University School of Medicine, Hangzhou, China.

<sup>7</sup>Hudson Institute of Medical Research, and Department of Molecular and Translational Science, Monash University, Clayton, Victoria, Australia.

\*Shared first authors

#Shared senior authors

Correspondence to: Rhys S Allan ([rallan@wehi.edu.au](mailto:rallan@wehi.edu.au)) and Stephen L Nutt ([nutt@wehi.edu.au](mailto:nutt@wehi.edu.au))

Ph: +61 3 9345 2322 fax: +61 3 9347 0852

Running title: A chromatin-independent role for Ezh2 in T cell development

Keywords: chromatin/Ezh2/lymphocyte/methylation/polycomb

## **Abstract**

Enhancer of Zeste 2 (Ezh2) mainly methylates lysine 27 of histone-H3 (H3K27me3) as part of the Polycomb repressive complex 2 (PRC2) together with Suz12 and Eed. However, Ezh2 can also modify non-histone substrates, although it is unclear if this mechanism has a role during development. Here, we present evidence for a chromatin-independent role of Ezh2 during T cell development and immune homeostasis. T cell-specific depletion of Ezh2 induces a pronounced expansion of natural killer T (NKT) cells, although Ezh2-deficient T cells maintain normal levels of H3K27me3, suggesting a chromatin-independent mechanism. In contrast, removal of Suz12 or Eed destabilizes canonical PRC2 function and ablates NKT cell development completely. We further show that Ezh2 directly methylates the NKT cell lineage defining transcription factor PLZF, leading to its ubiquitination and subsequent degradation. Sustained PLZF expression in Ezh2-deficient mice is associated with the expansion of a subset of NKT cells that cause immune perturbation. Taken together, we have identified a chromatin-independent function of Ezh2 that impacts on the development of the immune system.

## Introduction

Post-translational modifications to chromatin in the form of histone marks are known to be important for gene regulation. However, the enzymes that are responsible for laying down these marks can also modify non-histone proteins [1,2], making it important to understand whether such alternative mechanisms play a role in the regulation of cell fate. One of the key epigenetic silencing pathways involves the polycomb repressor complex 2 (PRC2) which consists of non-redundant components *Suppressor of zeste 12 homolog* (Suz12) and *Embryonic ectoderm development* (Eed) and the histone methyltransferase *Enhancer of zeste homolog 2* (Ezh2), which is responsible for the tri-methylation of lysine 27 of Histone-H3 (H3K27me3) [3]. Recently, it has been found that a homologue of Ezh2, Ezh1 can also impart H3K27me3 and compensate for the loss of Ezh2 in some circumstances [4-6].

Ezh2 has also been shown to methylate non-histone proteins such as transcription factors resulting in a range of outcomes, such as functional repression [7] and degradation [8]. Ezh2 methylation of Vav1 or talin has a role in actin polymerization [9] and cell migration [10], however the extent to which these events contribute to the differentiation of immune cells is unknown.

Here we examined whether there was a role for chromatin-independent functions of Ezh2 in T cell development. The process of T development occurs in the thymus where hematopoietic progenitors (known as thymocytes) develop into mature T cell lineages. Deletion of Ezh2 at this early point arrests T cell development [9,11]. The major T cell populations that arise are defined by the expression of either CD4 or CD8 molecules (known as co-receptors). These cells possess an  $\alpha\beta$  T cell receptor (TCR) that recognises peptides bound to class I or class II Major Histocompatibility Complex (MHC) molecules, respectively. The commitment to the

CD4 or CD8 T cell lineage occurs quite late in thymic development. Initially, precursors committed to the  $\alpha\beta$  lineage, which have rearranged genes encoding their TCR chains (TCR $\beta$  and TCR $\alpha$ ), transition through a stage known as double-positive (DP) where they express both the CD4 and CD8 co-receptors. They then undergo a selection phase where only cells with appropriate avidity for self-ligands survive and differentiate into mature T cells. It is at this stage that the choice of the CD4 or CD8 lineage is made. There are also “non-conventional” T cells that develop in the thymus such as  $\gamma\delta$  T cells and Natural Killer T (NKT) cells that are very important for innate responses. NKT cells develop during the DP stage and are a heterogeneous population of CD1d-restricted innate-like T cells that recognize glycolipid antigens and are potent and rapid producers of cytokines [12,13]. Due to their potency in producing a range of different cytokines NKT cell numbers must be kept in check as their aberrant expansion results in the activation of the adaptive immune system [14,15]. Thus, NKT cells have been implicated in a number of autoimmune diseases, such as asthma [16] and inflammatory bowel disease [17], as well as being targets for cancer immunotherapy [18]. NKT cells have their own distinct transcriptional profile [19] that depends on the master transcription factor promyelocytic leukaemia zinc finger (PLZF, encoded by *Zbtb16*) [20,21].

Here we identify a chromatin-independent role for Ezh2 in regulating T cell development and immune homeostasis. We observed Ezh2-deficiency results in the expansion of NKT cells that maintain normal levels of H3K27me3. In contrast, removal of the PRC2-core components Suz12 and Eed led to H3K27me3 depletion and a dramatic loss of NKT cells. We identified a specific lysine residue of PLZF (K430) that is a target of Ezh2-induced methylation leading to the ubiquitination and degradation of the protein. Overall we have demonstrated that Ezh2 can act in a chromatin-independent manner to control NKT cell

development and preserve immune homeostasis potentially by fine-tuning levels of PLZF, via methylation-dependent ubiquitinylation.

## Results

**A chromatin-independent role for Ezh2 in the development of NKT but not conventional  $\alpha\beta$  T cells.** To study the contribution of the PRC2 to T cell development we bred mice in which the exons of *Ezh2* [22], *Suz12* [23] or *Eed* [6] are flanked by *loxP* sequences to transgenic mice expressing cre recombinase under the control of the *Cd4* promoter [24], hereby referred to as conditional knock out ( $^{cKO}$ ) mice. We first confirmed deletion of the floxed alleles by PCR (Figure EV1a-c). We then examined the frequency of conventional  $\alpha\beta$  CD4<sup>+</sup> and CD8<sup>+</sup> T cells (Figure 1a) and  $\gamma\delta$  T cells (Figure 1b) in the thymus and spleen (not shown) of adult mice from all strains and found that they were similar to the wild type counterparts suggesting that removal of these components at the DP stage did not affect the subsequent development of these populations. However, using CD1d tetramers loaded with PBS57, a derivative of the glycolipid antigen  $\alpha$ -galactosyl ceramide (denoted NKT tetramer) we observed a large population of TCR $\beta$ <sup>+</sup> NKT cells in the thymus and spleen of the *Ezh2* $^{cKO}$  mice (Figure 1c; Figure EV2a and data not shown). This was in contrast to what was observed in the *Suz12* $^{cKO}$  and *Eed* $^{cKO}$  mice, which had a substantial loss of thymic NKT cells (Figure 1c; Figure EV2a). Thus we have revealed an unexpected difference in NKT cell development between mice deficient in *Ezh2* versus those deficient in the non-redundant components *Suz12* and *Eed*.

*Ezh2* is a histone methyltransferase, that, when in complex with its PRC2 cofactors *Suz12* and *Eed*, imparts the H3K27me3 mark that is associated with gene silencing [25]. Surprisingly, we did not observe a reduction of H3K27me3 levels in *Ezh2* $^{cKO}$  NKT cells when compared to wild type NKT cells by both flow cytometry and western blot (Figure 1d and e). The maintenance of H3K27me3 was most likely due to compensation by the closely related *Ezh1*, as has been shown in some other circumstances [4-6,26]. Consistent with this notion,

we found that Ezh1 was expressed in wild type NKT cells and that its expression increased in the *Ezh2<sup>ckO</sup>* cells (Figure 1d). This indicated that the canonical PRC2 function of laying down H3K27me3 occurred relatively normally and suggested that Ezh2 may control NKT cell development in a manner that is independent of its role as a chromatin-modifying enzyme. In support of this hypothesis, the removal of Suz12 and Eed which is known to compromise the ability of both Ezh2 and Ezh1 to methylate H3K27 [5,6] and lead to a loss of NKT cells resulted in a strong reduction in the levels of H3K27me3 (Figure 1f) suggesting that the PRC2 in these cells has been destabilized. Further evidence of PRC2 disruption comes from the fact that Ezh2 levels were substantially reduced in both the *Suz12* and *Eed<sup>ckO</sup>* thymocytes (Figure EV2b), whereas Suz12 levels were unaltered in the *Ezh2<sup>ckO</sup>* (Figure EV2c). In combination, this data indicates that the complete loss of the PRC2 function impairs NKT cell development, while the expansion of NKT cells in the absence of Ezh2 derives from the loss of a chromatin-independent function of this factor during NKT cell development.

**Ezh2-deficiency leads to the expansion of PLZF<sup>high</sup> NKT cells.** NKT cells arise from CD4<sup>+</sup>CD8<sup>+</sup> thymocytes and are thought to progress in a linear fashion from a CD24<sup>+</sup> CD44<sup>-</sup> NK1.1<sup>-</sup> population (known as stage 0), to stage 1 (CD24<sup>-</sup> CD44<sup>-</sup> NK1.1<sup>-</sup>), stage 2 (CD24<sup>-</sup> CD44<sup>+</sup> NK1.1<sup>-</sup>) and stage 3 (CD24<sup>-</sup> CD44<sup>+</sup> NK1.1<sup>+</sup>) [13]. Recently, an alternative model has been proposed, in which some stage 2 and 3 NKT cells diverge from a common stage 0 or 1 progenitor to take on different transcriptional and functional properties [14,27]. This has led to the demarcation of some cells in stages 1 and 2 as “NKT2” as these cells have more T helper 2 like properties (such as high IL4 production) and express high levels of the transcription factor PLZF and stage 3 as PLZF<sup>low</sup>Tbet<sup>high</sup> NKT1 for their functional similarity to T helper 1 cells [14,27]. To understand how Ezh2 regulates NKT cell development in a non-canonical fashion we sought to determine which stage of differentiation is affected by the

loss of Ezh2. Fractionation of the wild type and Ezh2-deficient thymi showed a large proportion of the NKT cells from the *Ezh2<sup>ckO</sup>* accumulated at stage 2 (Figure 2a) and expressed high levels of PLZF (Figure 2b) and IL4 (Figure EV3a). Moreover, NKT cells from the *Ezh2<sup>ckO</sup>* expressed low levels of Tbet and ROR $\gamma$ t (Figure EV3b) and thus could be considered akin to NKT2 cells.

To investigate the transcriptional changes that occurred in NKT cells lacking Ezh2 we employed RNAseq. We isolated stage 1, 2 and 3 NKT cell populations from wild type and *Ezh2<sup>ckO</sup>* thymocytes (sort profile shown in Figure EV2c). A comparison of wild type stage 1 vs stage 3 NKT cells yielded over 1500 differentially expressed genes (Figure 2c, Figure EV2d and Dataset 1) illustrating the dramatic transcriptional changes that parallel PLZF down regulation during NKT cell maturation. Surprisingly, we found only 297 up regulated and 62 down regulated genes in *Ezh2<sup>ckO</sup>* stage 2 NKT cells in comparison to their wild type counterparts (Figure 2c, Figure EV2d) and even fewer changes between the genotypes at stages 1 and 3 (Figure EV2e & f, Dataset 2). The relatively minor changes in gene up regulation in the absence of Ezh2 correlated with the unaffected levels of H3K27me3 (Figure 1d & e). Interestingly, we found that a number of genes that were down regulated in stage 2 *Ezh2<sup>ckO</sup>* NKT cells were Th1-type genes including *Tbx21* (encoding Tbet), *Ill8rap* and *Il2rb* (Figure 2c), genes which are highly expressed in the stage 3 population indicating that the loss of Ezh2 results in a block of cells at stage 2 or a skewing towards the NKT2 subset. Overall, this suggests that the loss of Ezh2 results in accumulation of stage 2/NKT2 type cells, and that development of these cells appears to be independent of conventional pathway of Ezh2-PRC2 gene silencing.

**PLZF is a target for Ezh2 methylation and degradation.** Recently it has been shown that Ezh2 can methylate transcription factors in a process that could alter their function or lead to their degradation [7,8,28]. As PLZF (encoded by the *Zbtb16* gene) is a master regulator of NKT cell development [20,21] and was highly expressed in the expanded population of *Ezh2<sup>CKO</sup>* NKT cells (Figure 2b) we investigated the possibility that it was the direct target of Ezh2. We confirmed previous reports that PLZF protein levels are dynamically regulated throughout normal NKT cell development, being high at stage 1 and reduced thereafter (Figure 3a) [20,29]. Strikingly, the down modulation of PLZF protein concentration during progression from stage 1 to 2 did not correlate with *Zbtb16* transcript abundance, which remained high at stage 2 (Figure 3b), suggesting that post-translational modifications regulate PLZF protein stability. In *Ezh2<sup>CKO</sup>* NKT cells high PLZF amounts were sustained in stage 2 (Figure 3c), although the transcript levels were equivalent in wild type and *Ezh2<sup>CKO</sup>* NKT cells (Figure 3d and e). We also found that the amount of H3K27me3 was very low at the *Zbtb16* promoter of both the WT and *Ezh2<sup>CKO</sup>* stage 2 NKT cells in comparison to that of *Hoxa11*, a gene known to be silenced in hematopoietic cells [30], providing more evidence for a chromatin-independent effect by Ezh2 on PLZF protein (Figure 3f).

PLZF stability is thought to be controlled by ubiquitin-mediated degradation [31] and recently PLZF has been shown to be associated with the E3 ligase cullin 3 in NKT cells [32], raising the possibility that Ezh2 methylase activity may directly control PLZF ubiquitination and degradation. Such a mechanism is not without precedence as Ezh2 establishes a “methyl-degron” on the transcription factor ROR $\alpha$  [8] (which was not differentially expressed in *Ezh2<sup>CKO</sup>* NKT cells; Figure EV4a). We firstly confirmed that PLZF was indeed methylated in NKT cells and that this methylation was reduced in the absence of Ezh2 (Figure EV4b). As NKT cells are a very rare population we characterized this mechanism further using the 293T

cell line. We found that indeed Ezh2 and PLZF could interact (Figure 4a & b). In addition, the presence of Ezh2 led to increased PLZF methylation (Figure 4c). Moreover, inhibition of Ezh2 methyltransferase activity using the small molecule inhibitor GSK126 [33] reduced PLZF methylation suggesting that the enzymatic activity of Ezh2 is critical in this process (Figure EV4c). Interestingly the presence of Suz12 was not required for this process as the knockdown of Suz12 expression (Figure EV4d), did not affect the levels of PLZF methylation in this system (Figure EV4e).

We then used a lysine methylation predicting tool [34] which highlighted K430 as a likely site for PLZF methylation ([bioinfo.ncu.edu.cn/inquiries\\_PMeS.aspx](http://bioinfo.ncu.edu.cn/inquiries_PMeS.aspx)). Interestingly this site is highly conserved across species (Figure EV4f). Substitution of K430 to arginine (R) resulted in almost complete loss of Ezh2-induced PLZF methylation (Figure 4c). When Ezh2 was introduced into cells that co-expressed PLZF and Ubiquitin-HA we observed strong ubiquitinylation of PLZF, which was lost in the K430R mutant (Figure 4d). This correlated with increased stability of K430R PLZF after blocking protein synthesis with cyclohexamide (Figure 4e). Moreover, knockdown of endogenous Ezh2 with siRNA (Figure EV4g) resulted in increased stability of WT PLZF (Figure 4f), which did not alter *Zbtb16* transcription (Figure EV4h). In combination, this data demonstrates that PLZF is a novel target of the Ezh2-methyl-degron.

We next examined the effect of mutating of the Ezh2 methylation site in PLZF on primary T cells. To this end, we produced retroviruses encoding WT PLZF or K430R PLZF and observed a statistically significant increase in the levels of PLZF in primary CD4<sup>+</sup> T cells carrying the K430R mutant (Figure EV5a). To determine if NKT cell differentiation was altered we transduced fetal liver stem cells with these vectors with the objective to

reconstitute the immune system of lethally irradiated recipient mice. Unfortunately we found that while we could obtain GFP<sup>+</sup> T cells infected with the empty vector we could not recover T cells that over-expressed either WT PLZF or PLZF K430R (data not shown). This suggests that PLZF introduction in stem cells restricts their ability to develop into T cells. Alternatively we introduced these vectors into thymic progenitors and studied NKT cell development *in vitro*. Introduction of K430R PLZF led to an increased proportion of cells at stage 1 and a corresponding decrease in stage 3 (Figure EV5b). Overall this data shows that Ezh2 can target PLZF for degradation and that mutating this target site stabilizes PLZF and alters NKT cell differentiation.

**PLZF<sup>high</sup> NKT cells are the cause of immune perturbation in *Ezh2<sup>CKO</sup>* mice.** Finally we studied how the loss of the Ezh2 affected immune homeostasis. Perturbations of CD8<sup>+</sup> T cell homeostasis by extrinsic factors, namely IL4[15], have been observed in mice lacking the tyrosine kinase Itk [35] and the transcription factors Klf2 [15] and Id3 [36] and have been attributed to the expansion of innate T cell populations such as NKT or  $\gamma\delta$  T cells [15]. A more detailed examination of the phenotypic characteristics of the T cells which developed in the absence of Ezh2 revealed a dramatic alteration specific to the activation status of the CD8<sup>+</sup>, but not the CD4<sup>+</sup> T cell population (Figure 5a & Figure EV5c). Ezh2-deficient CD8<sup>+</sup> T cells adopted memory-like characteristics including the up-regulation of CD44, expression of the transcription factor Eomes and the production of IFN $\gamma$ , yet they maintained expression of CD62L, indicative of a central memory phenotype (Figure 5a & b). In line with this we also found a dramatic increase in IL4-induced immunoglobulin E (IgE) in the serum of the *Ezh2<sup>CKO</sup>* mice (Figure 5d) as has been noted previously [37], suggesting that B cell homeostasis was also perturbed.

To investigate whether NKT cells were indeed the driver of the immune perturbation, we specifically removed them by generating *Ezh2<sup>CKO</sup>* mice that also lacked CD1d, which is required for NKT development [38]. Loss of NKT cells also resulted in restoration in the proportion of CD8<sup>+</sup> T cells with a memory phenotype to near wild type levels (Figure 5c). Furthermore, the increased serum IgE in *Ezh2<sup>CKO</sup>* mice was also dependent on the presence of NKT cells (Figure 5d) Thus, genetic ablation of Ezh2 in the T cell lineage resulted in expansion of PLZF<sup>high</sup> NKT cells that adversely impacted on adaptive immune cell homeostasis.

## Discussion

While chromatin-independent functions of Ezh2 have been reported previously, they are not known to impact on the differentiation of immune cells. By using a combination of PRC2-deficient mice we have identified that Ezh2 plays such an alternative role in the regulation of NKT cell development. The retention of H3K27me3 and the few derepressed genes in Ezh2-deficient NKT cells, while surprising, has been also observed in PRC2-target genes in stem cells [5,6] and correlates with the evidence showing that Ezh1 can compensate for the role of Ezh2 to methylate H3K27 [4,5]. In support of an unconventional role for Ezh2 in the regulation of immune homeostasis we showed that removal of the non-redundant components of PRC2, Suz12 and Eed, ablated NKT cell development and did not phenocopy Ezh2 deletion. Conversely, due to the profound defects in H3K27me3 and NKT cell survival without Suz12 or Eed, we cannot exclude the possibility that these factors are also involved in the methylation of PLZF as they have been shown to be required for non-histone methylation by Ezh2 [7,9], although our data suggest that Suz12 was not required for this process. Future work will investigate the composition of the complex required to induce PLZF methylation.

Non-histone methylation by Ezh2 results in range of outcomes for the target protein, such as repression [7] or activation of transcriptional activity [28]. The results we describe here the result of PLZF methylation are in line with the previously described Ezh2-dependent methyl degron [8]. In this case methylation of ROR $\alpha$  by Ezh2 was recognized DDB1-CUL4-associated factor 1 (DCAF1), which acted as an adaptor for the recruitment of a culin4 containing ubiquitin ligase complex. Interestingly, culin3 is highly expressed in immune cells and has recently been shown to interact with PLZF in NKT cells [32].

In the *Ezh2*-deficient NKT cells we observed high levels of PLZF that were not due to increased transcription and we identified PLZF as a novel substrate for the *Ezh2* methyl-degron. Our data suggests that the sustained high-concentration of PLZF observed in the absence of *Ezh2* may guide cells towards an NKT2 fate, either by diverting cells from stage 0/1 NKT progenitors or by stalling NKT2 from becoming NKT1. In line with this, *Tbx21* and its target genes *IL2rb* and *IL18ra* [39] were down regulated in stage 1 and 2 NKT cells lacking *Ezh2*. Interestingly, T-bet knockout mice have an accumulation of NKT2 cells [14,40] suggesting that a mutual antagonism may exist between PLZF and T-bet. We propose a working model, in which *Ezh2*-mediated degradation of PLZF guides thymic NKT development and specifically enables stage 3/NKT1 development. In the absence of *Ezh2*, PLZF levels are maintained, *Tbx21* is repressed and Stage 2/NKT2 cells accumulate, which subsequently perturbs the adaptive cells of immune system. This is supported by a recent study that showed that high levels of PLZF indeed push cells towards the NKT2 pathway [41]. This highlights the potential role of the *Ezh2* methyl-degron in the rapid degradation of transcription factor levels in allowing stage 2 cells to pass to the next stage of development where *Zbtb16* transcription is subsequently repressed. This mechanism adds an additional layer of regulation in cell fate determination that is most at play in the differentiation of many cell types.

To assess the functional relevance of the *Ezh2*-PLZF methyl-degron on NKT cell development we retrovirally introduced WT PLZF or PLZF K430R into developing thymic NKT cell cultures. These are technically challenging experiments with a range of variables. Nevertheless, we observed a skewing of the cells transduced with the K430R mutant towards stage 1 and a corresponding drop in the proportion of stage 3 NKT cells. This suggests that stabilizing PLZF does indeed alter NKT cell development, however, the modest effects

observed also imply that this mechanism may not be the only one operating in the expanded NKT cells from the *Ezh2<sup>cKO</sup>* mice. We speculate the Ezh2-PLZF methyl degron is required at the transition between stages 1 and 2 to downregulate PLZF protein prior to transcriptional repression of *Zbtb16* at stage 3, and that introducing this stabilized version of PLZF into early NKT cell progenitors (stage 0) may lead to the early block at stage 1.

Recently, the groups of Tarakhovsky and Bosselut also observed NKT cell expansion in *Ezh2<sup>cKO</sup>* mice, which they concluded, was caused by the loss of the canonical function of H3K27me3-associated repression of *Zbtb16* transcription [29]. Our data suggests that this is unlikely for a number of reasons. Firstly we showed that the complete loss of the PRC2 function in *Suz12* or *Eed<sup>cKO</sup>* mice impairs NKT cell development, suggesting that the expansion of NKT cells in the absence of Ezh2 derives from the loss of a chromatin-independent function of this factor during NKT cell development. Moreover, we found that the *Zbtb16* promoter in both wild type and *Ezh2<sup>cKO</sup>* stage 2 NKT cells contains low levels of H3K27me3 and unaltered gene transcription, making it highly unlikely that Ezh2-deficiency would result in de-repression of an already active gene. Although transcription is unaltered Ezh2-deficient NKT cells have sustain higher levels of PLZF implicating post-translational regulation of this protein.

In summary we propose that through its control of PLZF concentration, Ezh2 maintains NKT cell numbers at appropriate levels and facilitates immune homeostasis. We believe that our study establishes a paradigm for alternative roles of Ezh2 and non-histone methylation in the regulation of cell fate determination,

## Methods

**Mice.** *Ezh2*<sup>fl/fl</sup> mice [22], *Eed*<sup>fl/fl</sup> mice [6] and *Cd1d*<sup>-/-</sup> mice [42] were described previously. *Suz12*<sup>fl/fl</sup> mice were generated at the Walter and Eliza Hall Institute [23]. The floxed strains were crossed to *Cd4cre* mice [24]. All mice lines have been maintained on a C57BL/6 (Ly5.2) background and were used between 4 and 8 weeks of age and were age and sex matched. Animal experiments were in accordance with the guidelines of the Walter and Eliza Hall Institute Animal Ethics Committee.

**Plasmids.** The plasmid for expression of CFP-tagged PLZF and FLAG-tagged PLZF derivatives were generated by subcloning the human PLZF cDNA into pECFP-C1 or pCMV-Flag (Clontech Laboratories, Inc.) as described previously [43]. The Lenti ORF clone of Human EZH2 (Myc-Flag tagged) cDNA from OriGene Technologies. mCherry-tagged EZH2 was generated by subcloning into pmCherry-C1 (Clontech Laboratories, Inc.). All cDNA constructs were verified by DNA sequencing.

**Antibodies and flow cytometry.** Fluorochrome-conjugated antibodies against the following mouse antigens were used for analysis by flow cytometry: Brilliant Violet- or phycoerythrin-conjugated tetramers of CD1d containing the  $\alpha$ -GalCer derivative PBS57 were obtained from the Tetramer Core Facility of the US National Institutes of Health. CD4 (RM 4-5), CD62L (MEL-14), Ly5.2 (104), CD44 (IM7), IFN $\gamma$  (XMG1.2), T-bet (04-46), EZH2 (clone 11), Ror $\gamma$ t (Q31-378) from BD Pharmingen; CD8 (53-6.7), TCR $\beta$  (H57-597), Ly5.1 (A20), Eomes (Dan11mag), IL-4 (BVD6-24G2),  $\gamma\delta$ TCR (B 1.1), NK1.1 (PK136), Tbet (4B10) from eBioscience. Anti-Ror $\alpha$  antibodies were from Abcam. Anti-PLZF polyclonal antibody (sc-11146) from Santa Cruz, Anti-PLZF mAb (2A9), anti-Ezh1 and anti-H3K27me3 from EMD Millipore. Surface staining was carried out at 4°C for 30 mins. Intracellular staining was performed using eBioscience Foxp3 staining kit as per the manufacturer's protocol. Antibody stained cells were analysed using BD FACS Canto II or BD Fortessa1.

**Enrichment of NKT cells.** Anti-CD8 (clone 53-6.7, rat IgG, produced in house) antibody was used to deplete CD8<sup>+</sup> T cells and DP thymocytes from the thymi of 6-8 week old C57BL/6 mice. Briefly, single cell suspension of thymocytes was incubated with anti-CD8 antibody for 30 min at 4°C. Unbound antibody was washed and the antibody-coupled cells were incubated with BioMag Goat Anti-Rat IgG beads (Qiagen) to deplete CD8<sup>+</sup> T cells and

DP thymocytes. The CD4<sup>+</sup> T cell enriched fraction was further incubated with the Phycoerythrin (PE) conjugated NKT cell tetramer for 30 min at room temperature. Anti-PE micro beads (Miltenyi) were used to positively select the tetramer-coupled NKT cells.

**NKT cell cultures and retroviral infection.** Anti-CD8 (clone 53-6.7, rat IgG, produced in house) antibody was used to deplete CD8<sup>+</sup> T cells and DP thymocytes from the thymi of 6-8 week old C57BL/6 mice. Briefly, single cell suspension of thymocytes was incubated with anti-CD8 antibody for 30 min at 4°C. Unbound antibody was washed and the antibody-coupled cells were incubated with BioMag Goat Anti-Rat IgG beads (Qiagen) to deplete CD8<sup>+</sup> T cells and DP thymocytes. NK1.1<sup>-</sup> CD8<sup>-</sup> cells were FACsorted and cultured on OP9-DL1 in the presence of 5ng/mL of recombinant IL7 (Peprotech). After two days, these cells were spin infected at 37°C in the presence of polybrene with either empty GFP retrovirus, WT PLZF GFP or K430R PLZF GFP retrovirus. Five days later NKT-tetramer<sup>+</sup> cells were examined for the expression of CD44 and NK1.1 by flow cytometry.

**Chromatin immunoprecipitation (ChIP).** ChIP was performed following an adapted protocol by Upstate/Millipore. In brief, stage 2 NKT cells were isolated from the thymus and crosslinking was performed by addition of 1% formaldehyde at room temperature for 10 min, followed by sonication and immunoprecipitation with 10 µg of anti-H3K27me3 (Millipore). qPCR was performed using the following primers: *Zbtb16* (Forward: 5'-AGCCCTTGCCCTGTACAAAGA-3', Reverse: 5'-TGCCTCACCAACCTTTCTTC-3'), *Hoxa11* (Forward: 5'-AGGAGAAGGGGTTTCCTTCAA-3', Reverse: 5'-CTCCGCGGTTTGTCATAAT-3').

**Real-time PCR analysis.** Total RNA was prepared using RNeasy kit (Qiagen) from WT or *Ezh2*<sup>CKO</sup> NKT cells that were purified by flow cytometry. cDNA was made using iScript reverse transcription kit (Biorad) as per the manufacturers protocol. Real-time PCR was performed with the SYBR Green PCR kit (Bioline). Analyses were performed in triplicate and mean normalized expression was calculated with the Q-Gene application with *Gapdh* as the reference gene. The following primers were used: *Gapdh* (Forward: 5'-ACGGCCGCATCTTCTTGTGCA-3', Reverse: 5'-AATGGCAGCCCTGGTGACCA-3'), *Zbtb16* (Forward: 5'-GACGCACTACAGGGTTCACA-3', Reverse: 5'-CGTTGTGTGTTCTCAGGTGC-3').

**Immunoprecipitation and immunoblotting from NKT cells.** NKT-tetramer enriched thymocytes ( $1 \times 10^7$ ) were lysed with 0.5ml of lysis buffer (50mM Tris-HCl, pH 8.0, 150mM NaCl, 5mM EDTA, pH8.0, 0.5% (v/v) Nonidet P-40, 1mM dithiothreitol and 1X protease inhibitor mix (Roche) for 30 min on ice. Lysates were cleared by centrifugation, pre-cleared with Protein G Dynabeads (Invitrogen) for 1 hr at 4°C and incubated with anti-PLZF bound protein G Dynabeads for 12hrs at 4°C. Beads were washed thrice with cold lysis buffer followed by three washes with PBS and one wash with PBS with 0.05% TritonX100. Bound proteins were eluted by boiling the beads with 50µl of 2x Laemmli sample buffer. For immunoblotting whole cell extracts were prepared by lysing flow cytometrically sorted NKT cells in RIPA buffer (Millipore). Proteins were resolved in denaturing conditions in 4-12 % gradient SDS-PAGE (Life technologies) and were transferred onto nitrocellulose membrane (Biorad). Membrane was probed with following antibodies: mouse anti-PLZF (Santa Cruz), rabbit anti-Methyl-lysine (Abcam), rabbit anti-Ezh2 (Cell Signaling), rabbit anti-Suz12 (Cell Signaling), rabbit anti-Histone H3 (Cell Signaling) and goat anti-LaminB1 (Santa Cruz).

**Immunoprecipitation and Immunoblotting from 293T cells.** For the detection of PLZF ubiquitylation, cells were transfected with plasmids encoding PLZF-Flag and HA-Ub with either mCherry or Ezh2-mCherry. After incubation for 48 hours, cells were treated with 20 µM MG132 for 4 hours. Cells were then lysed with an NP40-containing lysis buffer and incubated with anti-Flag M2 antibodies. Antibody complexes were isolated with protein Affinity beads (Sigma-Aldrich), and immunocomplexes were run an SDS-PAGE gel. Ubiquitylated PLZF was visualized by immunoblotting with anti-HA antibody (Life Technologies).

For detection of PLZF lysine methylation, 293T cells were transfected with plasmids encoding Flag-PLZF with either mCherry or Ezh2-mCherry. After 48 hours, cells were lysed with an NP40-containing lysis buffer and incubated with anti-Flag M2 antibodies. Antibody complexes were isolated with protein Affinity beads (Sigma-Aldrich), and immunocomplexes were analyzed by SDS-PAGE and immunoblotting with anti-methylated lysine (Abcam) and anti-PLZF (Calbiochem). Inhibition of Ezh2 methyltransferase activity was performed by treating the cells with 10µM of GSK126 (selleck,S7061) for 48hrs.

For co-immunoprecipitation, 293T cells were transfected with plasmids encoding PLZF-Flag and Ezh2-mCherry or Ezh2-Flag and PLZF-CFP. After 48 hours, cells were lysed with an NP40-containing lysis buffer and incubated with anti-Flag M2 antibodies. Antibody complexes were isolated with protein Affinity beads (Sigma-Aldrich), and immunocomplexes

were analyzed by SDS-PAGE and immunoblotting with anti-Ezh2 and anti-PLZF. Protein bands were detected and quantified on a Li-Cor Odyssey infrared imaging system. To analyse protein stability, the PLZF and PLZF K430R plasmids were transfected into 293T cells which and after 24 hours were then treated with cycloheximide (20 ug/ml) and analyzed at the indicated times after treatment.

**Knock down of *Suz12*.** The MIT CRISPR design software was used for the design of sgRNAs (<http://crispr.mit.edu>). sgRNA sequence is as follows: SUZ12 exon 1: ACGGCTTCGGGCGCAAATC. Lentiviral particles were produced by transient transfection of 293T cells grown in 10 cm Petri dishes with 10 ug of vector DNA (containing pFgh1tUTG vector with target sgRNA inserted and the pFUCas9mCherry vector) along with the packaging constructs pMDL (5 ug), pRSV-rev (2.5 ug), and pVSV-G (3 ug) using standard calcium phosphate precipitation. Virus containing supernatants were collected at 48–72 hr after transfection and passed through a 0.45um filter. To establish Suz12 knockdown 293T cells treated with 8 ng/ml polybrene in the viral supernatant, incubated for 30 min at 37°C, and then centrifuged at 2,200 rpm for 2.5 hr at 32°C. Doxycycline hyclate (Sigma-Aldrich D9891) was used for treatment of cell lines to induce expression of the sgRNA for 3 days.

**Knockdown of *Ezh2* and assessment of PLZF stability.** Short hairpin RNA (sh)RNA-mediated silencing was performed by transfecting 293T cells with GIPZ Lentiviral Human shRNA vector for three different expressing 19 nucleotide shRNAs against EZH2 ( EZH2 target sequence TTAAGATTTCCGTTCTTTC, TATTGGTGTTTGACACCGA, TTATCATACACTTCCCTC). A non-targeting shRNA (ATCTCGCTTGGGCGAGAGTAAG) was used as negative control (Dharmacon, Thermo Fisher Scientific, Lafayette, CO). Samples were collected after cycloheximide (20 ug/ml) treatment at the indicated time to determine the protein levels of PLZF. EZH2 silencing in 293T cells was assessed by both Western blotting and qRT-PCR after 72h post-transfection.

**RNA-sequencing and bioinformatic analysis.** Thymocytes were isolated from wild type or *Ezh2*<sup>CKO</sup> mice and depleted of CD8<sup>+</sup> cells using magnetic beads coupled to an anti-CD8 antibody. NKT cells identified by CD1d-tetramer and TCRβ, were sorted into different stages using a BD Influx cell sorter to purity of typically >97% using CD44, NK1.1 and CD24 antibodies. RNA purification was performed following the manufacturer's protocol using the

RNAeasy Plus Mini Kit (Qiagen). RNA samples were sequenced at the Australian Genome Research Facility using the Illumina HiSeq sequencing system. An average of 30 million single-end 100 bp reads was obtained for each sample, split evenly over 4 technical replicates. Reads were aligned to the *mm10* build of the mouse genome using *subread* [44] with default parameters. Over 97% of reads were successfully aligned in each sample. Technical replicates for each sample were pooled into a single library. For each library, mapped reads with a mapping quality score greater than or equal to 30 were assigned to mouse genes in the NCBI RefSeq mouse annotation build 38 using *featureCounts* [45]. An average of 74% of mapped reads were counted into genes for each library.

Read counts for each gene were then used in a differential expression (DE) analysis using the *limma* and *edgeR* packages [46,47]. Lowly-expressed genes were first filtered out if the average log-count per million (as computed by the *aveLogCPM* function) was less than 1. Xist and any genes on the Y chromosome were also removed to eliminate sex effects. Normalization was performed using the TMM method [48] to remove composition bias between libraries. Counts were then log-transformed using the *voom* function [49]. A linear model was fitted to the log-counts using the computed precision weights. Sample variances for each gene were computed and shrunk towards a mean-variance trend using a robust empirical Bayes strategy [50]. For each contrast, a *p*-value was computed for each gene using the *treat* method [51] relative to a fold change threshold of 1.2. The Benjamini-Hochberg method was then applied to control the false discovery rate (FDR). DE genes were defined as those that were detected at a treat FDR of 10%.

MA plots were generated for each contrast by plotting the average log-count per million against the shrunken log-fold change for each gene. Briefly, each log-fold change was computed using the GLM framework in *edgeR* with a prior count of 3 [52].

**Statistics.** If not stated otherwise a student t test was performed to test for statistical significance; error bars denote mean  $\pm$  S.E.M.

## Acknowledgements

We thank David Tarlinton, Amanda Light, Simon Willis, Jane Visvader, Marnie Blewitt and Sarah Kinkel from the Walter and Eliza Hall Institute and Nicholas Williamson (Bio21 University of Melbourne) for technical assistance, advice and discussions. We also thank Alexander Tarakhovsky (Rockefeller University) for the *Ezh2<sup>fl/fl</sup>* mice and Stuart Orkin

(DFCI, Harvard) for the *Eedfl/fl* mice. This work was supported by grants and fellowships from the National Health and Medical Research Council of Australia (RSA, SLN, WSA, GKS, AK, BRGW, DX, DIG), the Australian Research Council (RSA, SLN, AK), the Sylvia and Charles Viertel Foundation (AK), an American Asthma Foundation Grant (SLN, RSA), the National Natural Science Foundation of China (DX) (81273247, 81472655 and 31670905), the National Basic Research Program of China (2012CB911204) and the Netherlands Organization for Scientific Research (KPIvG). This study was made possible through Victorian State Government Operational Infrastructure Support and Australian Government NHMRC Independent Research Institute Infrastructure Support scheme and the Australian Cancer Research Fund.

### **Author contributions**

A.V. designed the research, performed experiments, analysed data and wrote the paper. D.X. designed the research, performed experiments and analysed data. K.P.J.M.vG., N.I., L.Y., and D.W. performed experiments and analysed data. A.L. and G.K.S. performed bioinformatics analysis. B.R.G.W, D.I.G and A.K., helped to design experiments and provided critical reagents. M.J.H. and A.J.K. generated critical reagents. S.C.W.L., I.J.M., and W.S. developed and characterized the *Suz12fl/fl* mice. S.L.N. and R.S.A. designed and supervised the research and wrote the paper.

### **Conflict of interest statement**

The authors have no competing conflicts of interest.

## References

1. Zhang X, Wen H, Shi X (2012) *Acta biochimica et biophysica Sinica* **44**: 14-27
2. Roth SY, Denu JM, Allis CD (2001) *Annual review of biochemistry* **70**: 81-120
3. Margueron R, Reinberg D (2011) *Nature* **469**: 343-349
4. Margueron R, Li G, Sarma K, *et al.* (2008) *Mol Cell* **32**: 503-518
5. Shen X, Liu Y, Hsu YJ, *et al.* (2008) *Mol Cell* **32**: 491-502
6. Xie H, Xu J, Hsu JH, *et al.* (2014) *Cell stem cell* **14**: 68-80
7. He A, Shen X, Ma Q, *et al.* (2012) *Genes Dev* **26**: 37-42
8. Lee JM, Lee JS, Kim H, *et al.* (2012) *Mol Cell* **48**: 572-586
9. Su IH, Dobenecker MW, Dickinson E, *et al.* (2005) *Cell* **121**: 425-436
10. Gunawan M, Venkatesan N, Loh JT, *et al.* (2015) *Nat Immunol* **16**: 505-516
11. Simon C, Chagraoui J, Krosli J, *et al.* (2012) *Genes Dev* **26**: 651-656
12. Godfrey DI, Stankovic S, Baxter AG (2010) *Nat Immunol* **11**: 197-206
13. Bendelac A, Savage PB, Teyton L (2007) *Annu Rev Immunol* **25**: 297-336
14. Lee YJ, Holzapfel KL, Zhu J, *et al.* (2013) *Nat Immunol* **14**: 1146-1154
15. Weinreich MA, Odumade OA, Jameson SC, *et al.* (2010) *Nat Immunol* **11**: 709-716
16. Umetsu DT, DeKruyff RH (2006) *Nature reviews. Immunology* **6**: 953-958
17. Olszak T, An D, Zeissig S, *et al.* (2012) *Science* **336**: 489-493
18. Mattarollo SR, Smyth MJ (2013) *Oncoimmunology* **2**: e22615
19. Cohen NR, Brennan PJ, Shay T, *et al.* (2013) *Nat Immunol* **14**: 90-99
20. Kovalovsky D, Uche OU, Eladad S, *et al.* (2008) *Nat Immunol* **9**: 1055-1064
21. Savage AK, Constantinides MG, Han J, *et al.* (2008) *Immunity* **29**: 391-403
22. Su IH, Basavaraj A, Krutchinsky AN, *et al.* (2003) *Nat Immunol* **4**: 124-131
23. Lee SC, Miller S, Hyland C, *et al.* (2015) *Blood* **126**: 167-175
24. Lee PP, Fitzpatrick DR, Beard C, *et al.* (2001) *Immunity* **15**: 763-774
25. Cao R, Wang L, Wang H, *et al.* (2002) *Science* **298**: 1039-1043
26. Ezhkova E, Lien WH, Stokes N, *et al.* (2011) *Genes Dev* **25**: 485-498
27. Constantinides MG, Bendelac A (2013) *Current opinion in immunology* **25**: 161-167
28. Kim E, Kim M, Woo DH, *et al.* (2013) *Cancer Cell* **23**: 839-852
29. Dobenecker MW, Kim JK, Marcello J, *et al.* (2015) *J Exp Med* **212**: 297-306
30. Heng TS, Painter MW, Immunological Genome Project C (2008) *Nat Immunol* **9**: 1091-1094
31. Sobieszczuk DF, Poliakov A, Xu Q, *et al.* (2010) *Genes Dev* **24**: 206-218
32. Mathew R, Seiler MP, Scanlon ST, *et al.* (2012) *Nature* **491**: 618-621
33. McCabe MT, Ott HM, Ganji G, *et al.* (2012) *Nature* **492**: 108-112
34. Shi SP, Qiu JD, Sun XY, *et al.* (2012) *PloS one* **7**: e38772
35. Atherly LO, Lucas JA, Felices M, *et al.* (2006) *Immunity* **25**: 79-91
36. Vervakakis M, Boos MD, Bendelac A, *et al.* (2010) *Immunity* **33**: 203-215
37. Tumes DJ, Onodera A, Suzuki A, *et al.* (2013) *Immunity* **39**: 819-832
38. Chen YH, Chiu NM, Mandal M, *et al.* (1997) *Immunity* **6**: 459-467
39. Jenner RG, Townsend MJ, Jackson I, *et al.* (2009) *Proc Natl Acad Sci U S A* **106**: 17876-17881
40. Townsend MJ, Weinmann AS, Matsuda JL, *et al.* (2004) *Immunity* **20**: 477-494
41. Pobezinsky LA, Etzensperger R, Jeurling S, *et al.* (2015) *Nat Immunol* **16**: 517-524
42. Sonoda KH, Exley M, Snapper S, *et al.* (1999) *J Exp Med* **190**: 1215-1226
43. Xu D, Holko M, Sadler AJ, *et al.* (2009) *Immunity* **30**: 802-816
44. Liao Y, Smyth GK, Shi W (2013) *Nucleic acids research* **41**: e108
45. Liao Y, Smyth GK, Shi W (2014) *Bioinformatics* **30**: 923-930
46. Ritchie ME, Phipson B, Wu D, *et al.* (2015) *Nucleic acids research* **43**: e47

47. Robinson MD, McCarthy DJ, Smyth GK (2010) *Bioinformatics* **26**: 139-140
48. Robinson MD, Oshlack A (2010) *Genome biology* **11**: R25
49. Law CW, Chen Y, Shi W, *et al.* (2014) *Genome biology* **15**: R29
50. Phipson B, Lee, S, Majewski, IJ, Alexander, WS, and Smyth, GK. (2016) *Annals of Applied Statistics* **10**: 946-963
51. McCarthy DJ, Smyth GK (2009) *Bioinformatics* **25**: 765-771
52. McCarthy DJ, Chen Y, Smyth GK (2012) *Nucleic acids research* **40**: 4288-4297

## Figure Legends

**Figure 1. Contrasting outcomes on NKT cell development upon deletion of individual PRC2 components.** Flow cytometric analysis of 6 week old wild type (WT) and *Ezh2<sup>ckO</sup>*, *Suz12<sup>ckO</sup>* or *Eed<sup>ckO</sup>* thymii showing proportion of (a) TCR $\beta^+$  CD4 and CD8 expressing T cells, (b) TCR $\beta^-$  TCR $\gamma\delta^+$  T cells, or (c) TCR $\beta^+$  PBS-57<sup>+</sup> NKT cells. Numbers are the mean percentage in the indicated gate. Data is representative of two independent experiments. (d) Histogram overlay shows flow cytometric analysis of H3K27me3 (left panel) and Ezh1 (right panel) levels in wild type (WT) and indicated genotypes in thymic NKT cells. Grey shaded histogram represents isotype control. (e) Lysates of TCR $\beta^+$  PBS-57<sup>+</sup> NKT cells derived from WT or from 5 individual *Ezh2<sup>ckO</sup>* mice were immunoblotted with antibodies specific for H3K27me3 or total histone-H3 as a loading control. (f) Histogram overlay shows flow cytometric analysis of H3K27me3 (left panel) and Ezh1 (right panel) levels in wild type (WT) and indicated genotypes in thymic NKT cells. Grey shaded histogram represents isotype control. Data in (a-f) is representative of at least 2 independent experiments.

**Figure 2. Ezh2 restricts the development of Stage 2 NKT cells.** (a) Flow cytometric analysis showing expansion of stage 2 NKT cells in *Ezh2<sup>ckO</sup>* mice. Left panel shows expression of NK1.1 and CD44 in WT (left) and *Ezh2<sup>ckO</sup>* (right) NKT cells from the thymus. Numbers are the percentage cells in the indicated quadrant. NKT cells corresponding to Stage (S) 1, 2 and 3 are indicated on the plots. Bar graph represents the mean percentage of NKT cells in each stage  $\pm$  S.E.M. (b) Contour plots show the expression of NK1.1 and PLZF. Graph shows the percentage of PLZF<sup>+</sup> NKT cells in both genotypes. Each dot represents an individual mouse, horizontal lines show the mean  $\pm$  S.E.M. NKT cells in the plots in (a) and (b) were identified by binding to TCR $\beta$  and the NKT-tetramer and are representative of at least two independent experiments. (c) RNAseq analysis of differential gene expression in wild type (WT) and *Ezh2<sup>ckO</sup>* NKT cells (False discovery rate  $\leq 0.1$  relative to 1.2-fold threshold). Left panel shows comparison of gene expression profiles from WT and *Ezh2<sup>ckO</sup>* stage 2 NKT cells. Right panel shows comparison of gene expression profiles from WT Stage 1 and Stage 3 NKT cells. In the left panel the blue and red dots represent genes that were significantly up or down regulated respectively in the *Ezh2<sup>ckO</sup>* compared to WT with specific examples highlighted. In the right panel, blue and red dots represent genes significantly up or down regulated in Stage 3 compared to stage 1 WT NKT cells respectively. In both graphs the

mRNA corresponding to the NKT cell specific transcription factor PLZF (*Zbtb16*) is marked to illustrate its stage specific expression pattern.

**Figure 3. Sustained expression of PLZF in Ezh2-deficient NKT cells is not associated with gene de-repression** (a) WT thymic NKT cells were analyzed for stage specific expression of PLZF protein by flow cytometry. (b) Quantitative real time PCR analysis of *Zbtb16* mRNA (encoding PLZF) in different stages of WT thymic NKT cells. Data are the mean  $\pm$  S.E.M from 2 experiments. (c) Flow cytometric analysis of PLZF expression in WT and *Ezh2*<sup>CKO</sup> stage 1 (left), stage 2 (middle) and stage 3 (right) NKT cells. (d) Bar graph shows expression of *Zbtb16* in WT and *Ezh2*<sup>CKO</sup> stage 2 NKT cells. Error bars represent  $\pm$  SEM from 3 independent experiments. (e) RNAseq track showing read mapping to the *Zbtb16* gene in WT and *Ezh2*<sup>CKO</sup> from stage 1-3 NKT cells. (f) ChIP enrichment of H3K27me3 at the transcriptional start site of *Zbtb16* and *HoxA11* from stage 2 NKT cells of the indicated genotypes. NKT cells stages were defined as shown in Supplementary Figure 1d. Data is representative of at least two independent experiments. NS, not significant (P>0.05).

**Figure 4. An Ezh2 methyl-degron regulates PLZF stability.** (a) Interaction between Ezh2 and PLZF. 293T cells were co-transfected with Ezh2-mCherry and PLZF-Flag expressing plasmids. Whole cell lysates were immunoprecipitated (IP) with anti-FLAG or control IgG antibodies and then immunoblotted (IB) with Ezh2 and PLZF-specific antibodies. 10% of total lysate was loaded as input. (b) 293T cells were co-transfected with Ezh2-Flag and PLZF-CFP expressing plasmids. Whole cell lysates were immunoprecipitated (IP) with anti-Flag or control IgG antibodies and then immunoblotted (IB) with PLZF and Ezh2-specific antibodies. 10% of total lysate was loaded as input. (c) Detection of Ezh2-dependent methylation of PLZF by immunoblot of lysates from 293T cells co-transfected with control (mCherry) or mCherry-Ezh2 and Flag-PLZF-expressing (WT or K430R) plasmids, whole cell lysates were immunoprecipitated with an anti-Flag antibodies and probed with methylated lysine and PLZF-specific antibodies. (d) Ezh2 induces the ubiquitinylation of PLZF. Plasmids encoding PLZF-Flag or PLZF K430R-Flag, and Ubiquitin-HA were transfected with mCherry or Ezh2-mCherry into 293T cells for 48 hours followed by IP of Flag-tagged PLZF. Cells were treated with 20mM MG132 for 4 hours prior to lysis. Western blotting was performed with antibodies specific for HA (to examine ubiquitinylation status of PLZF) and anti-PLZF to determine input. (e) The stability of WT or K430 PLZF was assessed in 293T cells at the

indicated times after blocking protein synthesis with cyclohexamide (CHX). **(f)** The stability of WT PLZF was assessed in 293T cells after knockdown of endogenous *Ezh2* by two independent shRNAs and culture in the presence of CHX for the indicated timepoints. Data are representative of at least two independent experiments.

**Figure 5. Loss of Ezh2 results in immune perturbation due to expansion of NKT cells**

**(a)** Wild type (WT) and *Ezh2<sup>ckO</sup>* splenic CD8<sup>+</sup> T cells were analyzed for central memory (CM) phenotype by flow cytometry. Top panel shows CD44 and CD62L expression by wild type (WT, left) and *Ezh2<sup>ckO</sup>* (right) CD8<sup>+</sup> T cells. Eomes expression by WT (left) and *Ezh2<sup>ckO</sup>* (right) CD8<sup>+</sup> T cells is shown in the bottom panel. Graph shows percentage of CD44<sup>+</sup>CD62L<sup>+</sup> of the total CD8<sup>+</sup> T cells from mice of the indicated genotypes. Data is from two independent experiments. **(b)** Representative profile and bar graph of the percentage of WT and *Ezh2<sup>ckO</sup>* CD8<sup>+</sup> T cells that were positive for intracellular IFN $\gamma$  after PMA/Ionomycin stimulation for 3 hrs. Data is pooled from two independent experiments and error bars represent  $\pm$  SEM from 4 individual mice. **(c)** Loss of NKT cells restores *Ezh2<sup>ckO</sup>* CD8<sup>+</sup> T cell phenotype to near wild type levels. Left panels show expression of CD44 and CD62L on CD8<sup>+</sup> T cells of the indicated genotypes. Graph shows percentage of CD44<sup>+</sup>CD62L<sup>+</sup> of the total CD8<sup>+</sup> T cells from mice of the indicated genotypes. Symbols in graphs indicate data points for individual mice from three independent experiments and horizontal lines indicate  $\pm$  S.E.M. **(d)** Bar graph showing ELISA measurement of serum IgE levels in indicated genotypes. Data is one representative of two independent experiments  $\pm$  SEM from 4 individual mice. Numbers in the plots in (a) and (b) are the percent cells in the indicated quadrant or gate.

## Expanded View Figure Legends

**Figure EV1. Deletion of floxed sequences from *cKO* mice.** PCR was performed on CD4<sup>+</sup>CD8<sup>+</sup> double positive (DP) thymocytes or CD19<sup>+</sup> splenic B cells from either WT (B6) or the indicated *cKO* genotype. Primers flanking the floxed sequences of *Ezh2* (a), *Suz12* (b) or *Eed* (c) were used. Annotation indicates the expected WT, floxed or deleted band sizes.

**Figure EV2. Expanded *Ezh2*-deficient NKT cells and levels of individual PRC2 components in thymocytes.** (a) Analysis of thymocytes from WT (littermate) and *cKO* of the indicated genotypes showing proportion (left panel) and total number of NKT cells (right panel). Symbols in graphs indicate data points for individual mice from two independent experiments and horizontal lines indicate  $\pm$  S.E.M. (b) Lysates of CD4<sup>+</sup>CD8<sup>+</sup> thymocytes derived from WT or the indicated *cKO* mice were immunoblotted with antibodies specific for *Ezh2* or total LaminB1 as a loading control. (c) Lysates of CD4<sup>+</sup>CD8<sup>+</sup> thymocytes derived from WT or *Ezh2*<sup>*cKO*</sup> mice were immunoblotted with antibodies specific for *Suz12* or total Histone-H3 as a loading control.

**Figure EV3. Expanded *Ezh2*-deficient NKT cells that express high amounts of PLZF are associated with increased frequencies of stage 2/NKT2 cells.** (a) Thymic WT and *Ezh2*<sup>*cKO*</sup> NKT cells (NKT-tetramer<sup>+</sup>) were examined for the expression of PLZF and IL-4 (after 3hrs of PMA/Ionomycin stimulation). (b) Analysis of NKT cell subsets from the thymus of WT and *Ezh2*<sup>*cKO*</sup> by flow cytometry. NKT-tetramer<sup>+</sup> and TCR $\beta$ <sup>+</sup> NKT cells were examined for the expression of PLZF, Tbet and Ror $\gamma$ t which allows cells to be defined as NKT1 (Tbet<sup>high</sup>, PLZF<sup>int</sup>), NKT2 (Tbet<sup>low</sup>, PLZF<sup>high</sup>) and NKT17 (PLZF<sup>int</sup>, Ror $\gamma$ t<sup>high</sup>). Lower panels show expression of CD44 and NK1.1 on NKT1, 2 and 17. Numbers are the proportion of cells in each gate. Graph shows the mean percentage of NKT1/2/17 cells  $\pm$ S.E.M. for both genotypes. Symbols in graphs indicate data points for individual mice from three independent experiments and horizontal lines indicate the mean  $\pm$  S.E.M. NS, not significant (P>0.05). Expression of CD44 and NK1.1 on NKT1, 2 and 17 gated as above. (c) Flow cytometry sorting profiles used to purify thymic NKT cells for RNA sequencing. Left panel shows Stage 3 NKT cells based on CD44 and NK1.1 expression. Right panel shows NKT cell stages 0-2 based on CD44 and CD24 expression on NK1.1<sup>-</sup> cells. (d) Bar graphs represent differentially expressed genes comparing between WT stages (left graph) or WT vs *Ezh2*<sup>*cKO*</sup> (false

discovery rate 0.1 relative to 1.2-fold threshold). **(e)** Comparison of WT and *Ezh2<sup>CKO</sup>* gene expression profiles of stage 1 (left) and stage 3 (right) NKT cells. The blue and red dots represent genes significantly up or down regulated respectively in the *Ezh2<sup>CKO</sup>* compared to WT. In both graphs the mRNA corresponding to the NKT cell specific transcription factor PLZF (*Zbtb16*) is marked to illustrate its stage specific expression pattern.

**Figure EV4. Characterization of PLZF methylation by Ezh2.** **(a)** Flow cytometric analysis of ROR $\alpha$  expression in WT and *Ezh2<sup>CKO</sup>* thymic NKT cells. Grey histogram is isotype control. **(b)** Protein extracts from NKT cell-enriched WT and *Ezh2<sup>CKO</sup>* thymocytes were immunoprecipitated with anti-PLZF and subjected to western blotting for PLZF (upper panel) and the corresponding lysine methylation (lower panel). Data is representative of four independent experiments. **(c)** Detection of Ezh2-dependent methylation of PLZF by immunoblot of lysates from 293T cells co-transfected with mCherry-Ezh2 and Flag-PLZF-expressing plasmids, whole cell lysates were immunoprecipitated with anti-Flag antibodies and probed with methylated lysine and PLZF-specific antibodies. Samples were either treated with vehicle control (-) or the Ezh2-specific inhibitor GSK126 (+). **(d)** Assessment of Suz12 levels by western blot in cell lysates derived from either control 293T cells or cells infected with a dox-inducible Suz12 targeting sgRNA and treated doxycycline.  $\beta$ -tubulin was used as a loading control. **(e)** Assessment of Ezh2 methylation of PLZF by immunoblot of lysates from either control 293T cells or Suz12 knockdown (Suz12 sgRNA) co-transfected with mCherry-Ezh2 and Flag-PLZF-expressing plasmids, whole cell lysates were immunoprecipitated with anti-Flag antibodies and probed with methylated lysine and PLZF-specific antibodies. **(f)** Conservation of PLZF K430 in the indicated species. **(g)** Assessment of knockdown of Ezh2 by shRNA by western blot in 293T cells.  $\beta$ -actin acts as a control for equal protein loading. **(h)** Quantitative real time PCR analysis of *Zbtb16* mRNA in 293T cells that have been transfected with WT PLZF plasmid and different shRNAs to knockdown *Ezh2*. *Zbtb16* expression was normalized to *Hprt*. Data are the mean  $\pm$ S.E.M. from 2 experiments.

**Figure EV5. Overexpression of K430R PLZF alters NKT cell development *in vitro*.**

**(a)** FACS analysis of PLZF levels in GFP<sup>+</sup> CD4<sup>+</sup> T cells overexpressing empty, PLZF WT or PLZF K430R constructs. Mean fluorescence intensity of PLZF levels on GFP<sup>+</sup> gated cells  $\pm$  S.E.M from two independent experiments is shown on right panel (normalized to WT). **(b)** Overexpression of PLZF K430R in thymic NKT cell cultures lead to an increased proportion

of stage 1 NKT cells. CD8<sup>-</sup> NK1.1<sup>-</sup> thymocytes were cultured on OP9-DL1 stromal cells in the presence of IL7 for two days prior to retroviral transfection with either empty, PLZF WT or PLZF K430R GFP virus. Five days later NKT-tetramer<sup>+</sup> GFP<sup>+</sup> cells were examined for the expression of CD44 and NK1.1. Graphs show the percent of cells in each stage of NKT development cells from four independent experiments  $\pm$  S.E.M. (c) Analysis of CD44 and CD62L expression by WT and *Ezh2*<sup>CKO</sup> CD4<sup>+</sup> T cells from spleen by flow cytometry. Data is representative of two independent experiments.

**Dataset 1.** RNAseq data comparisons of wild type NKT cell stages.

**Dataset 2.** RNAseq data comparisons of wild type vs *Ezh2*<sup>CKO</sup> NKT cell stages.

Figure 1

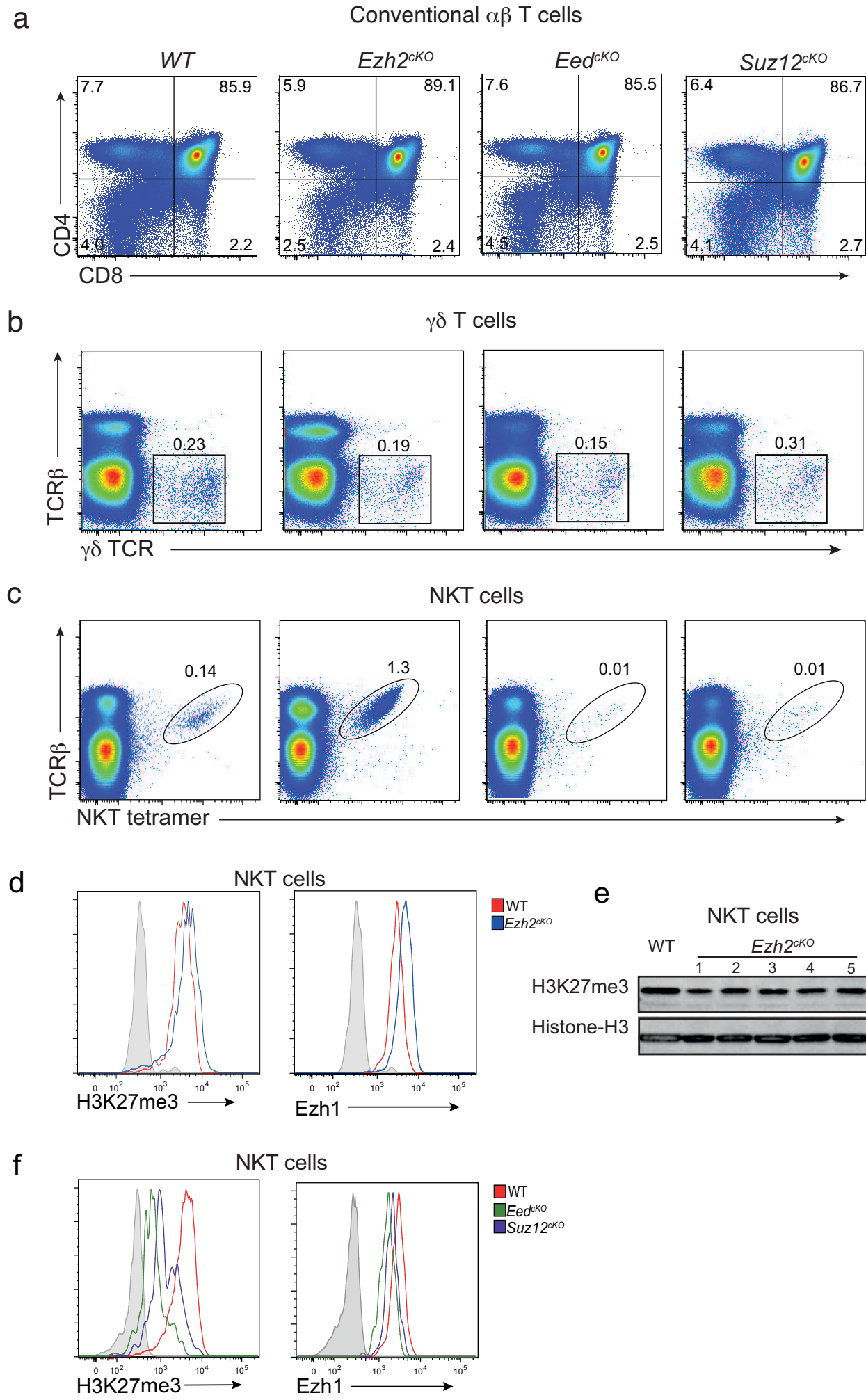


Figure 2

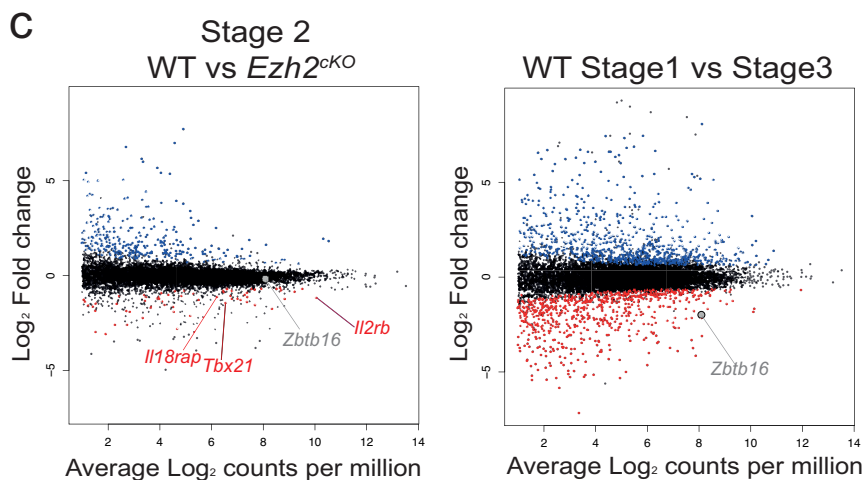
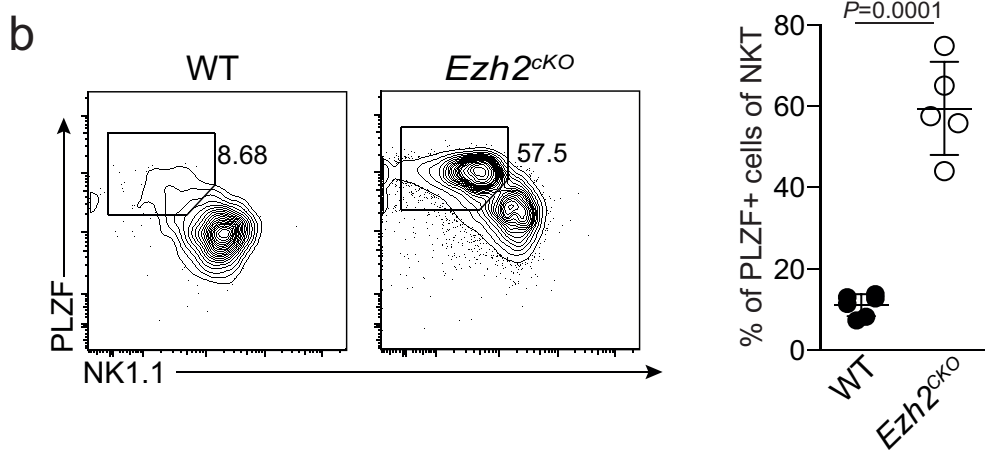
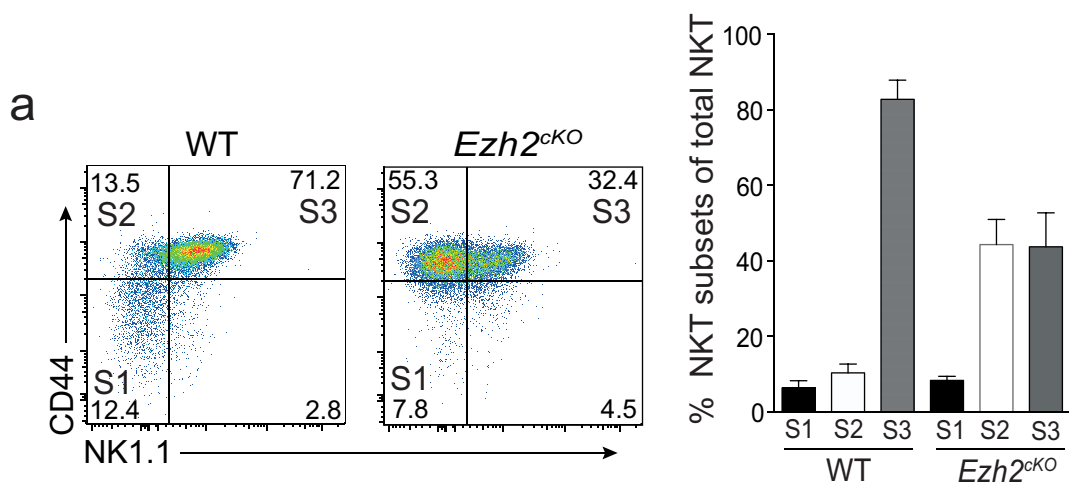


Figure 3

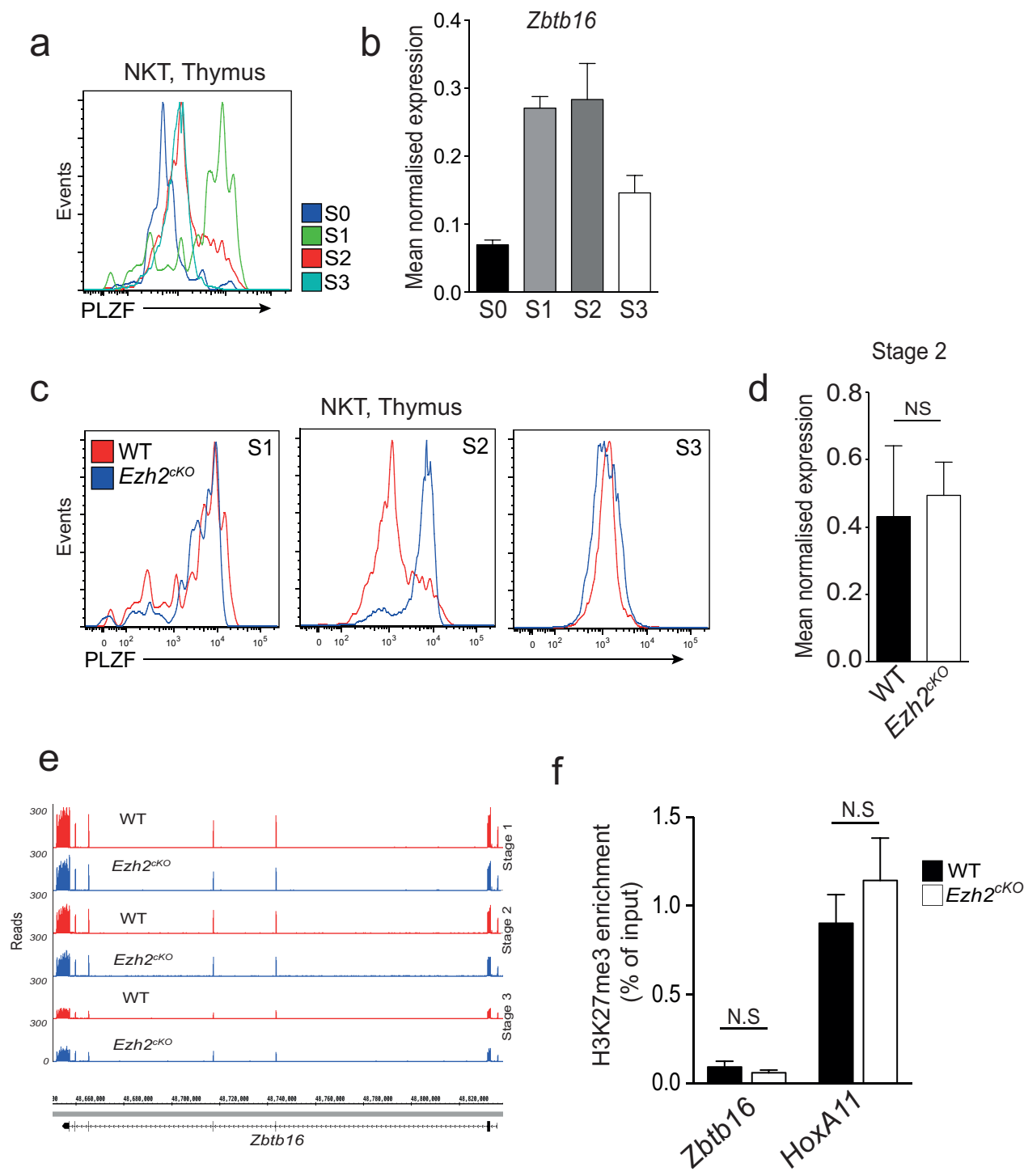




Figure 5

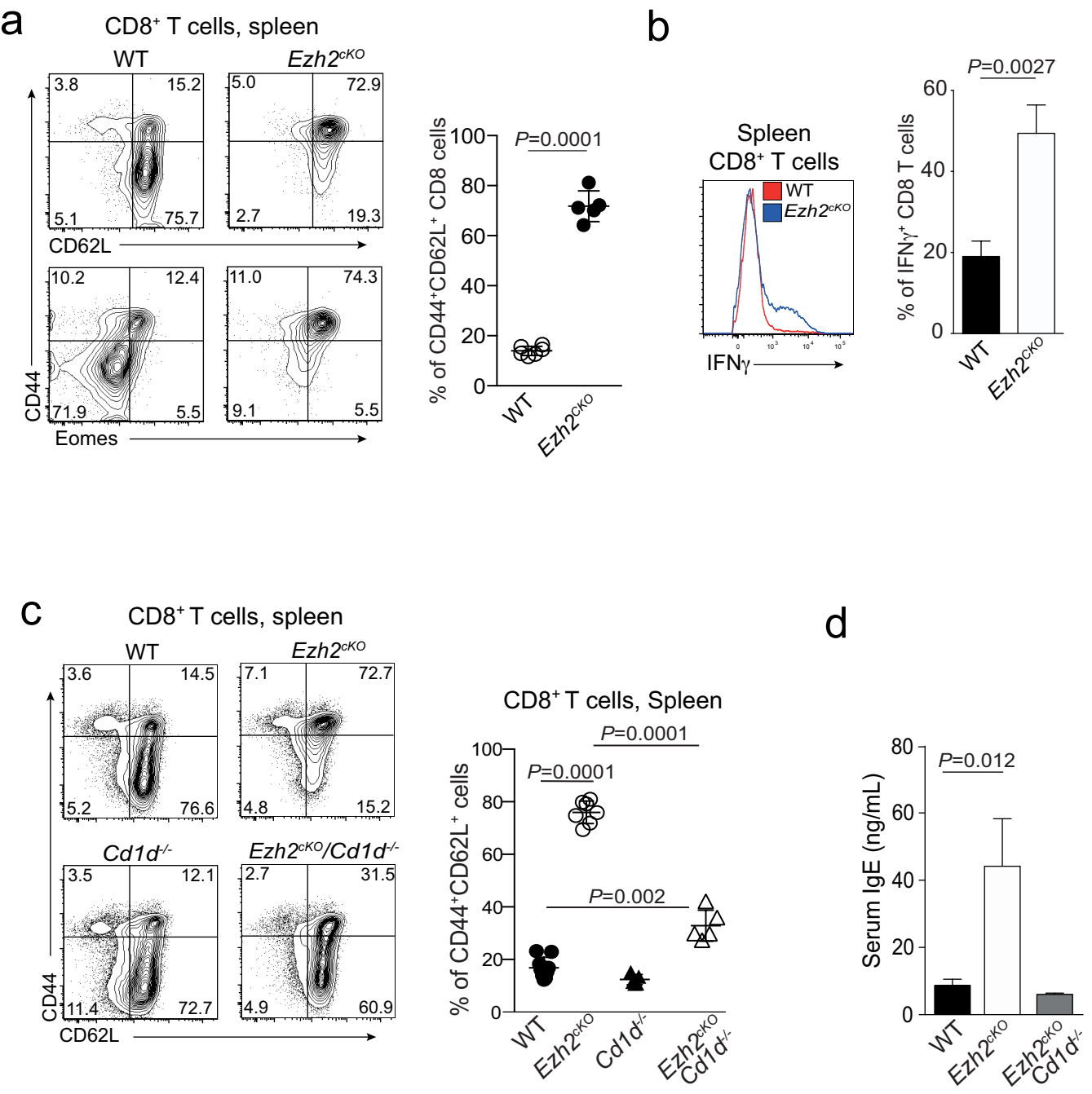
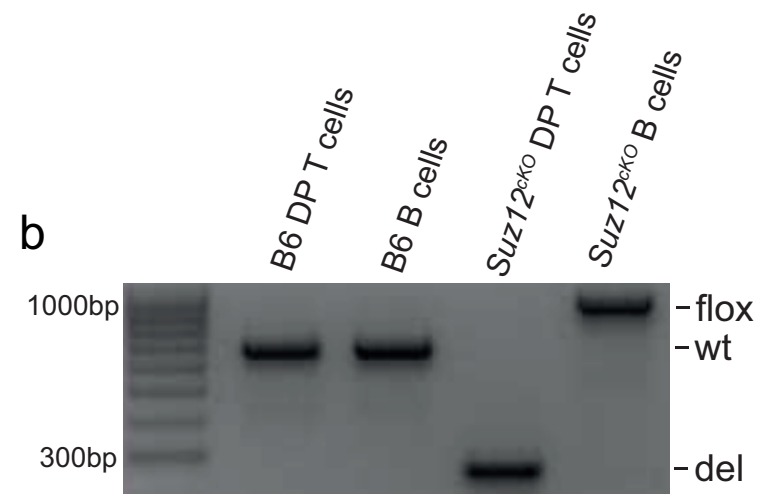


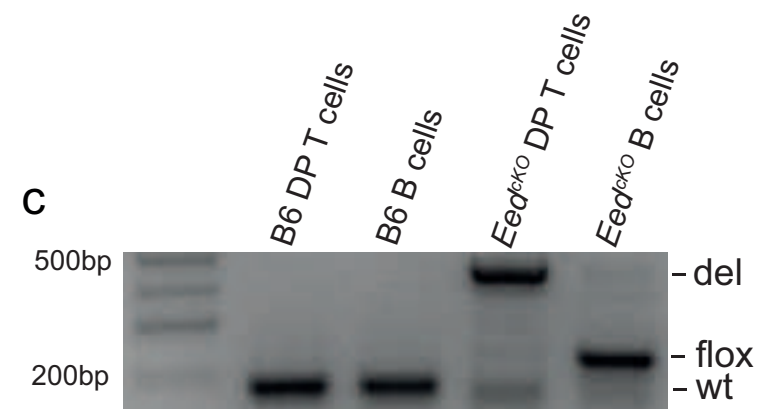
Figure EV1



*Ezh2*



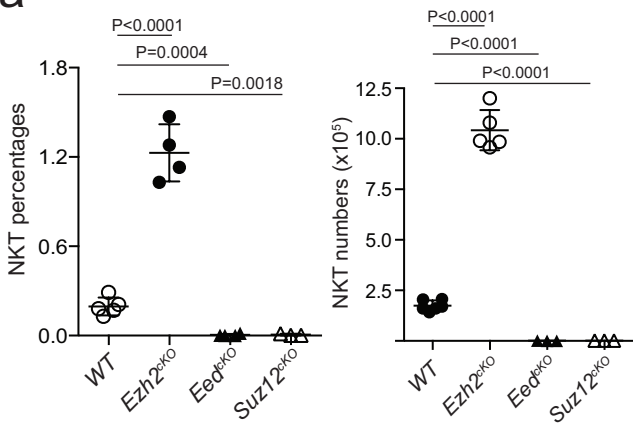
*Suz12*



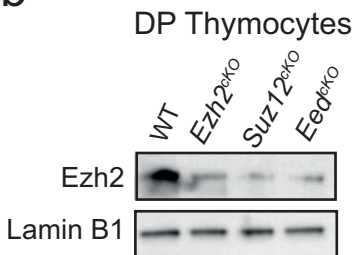
*Eed*

# Figure EV2

**a**



**b**



**c**

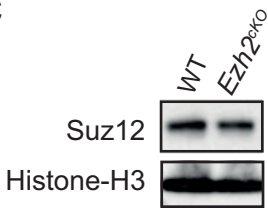


# Figure EV3

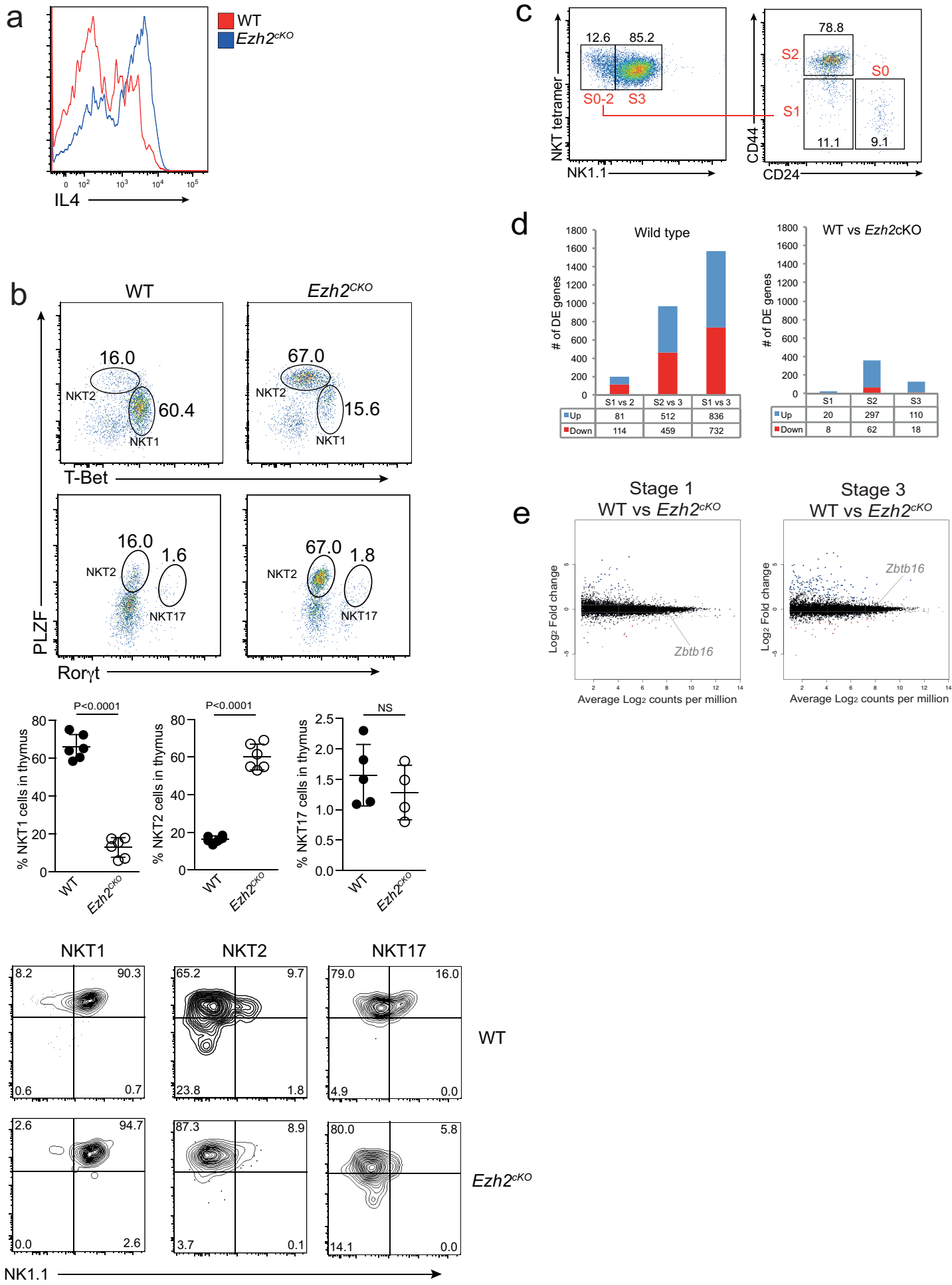


# Figure EV4

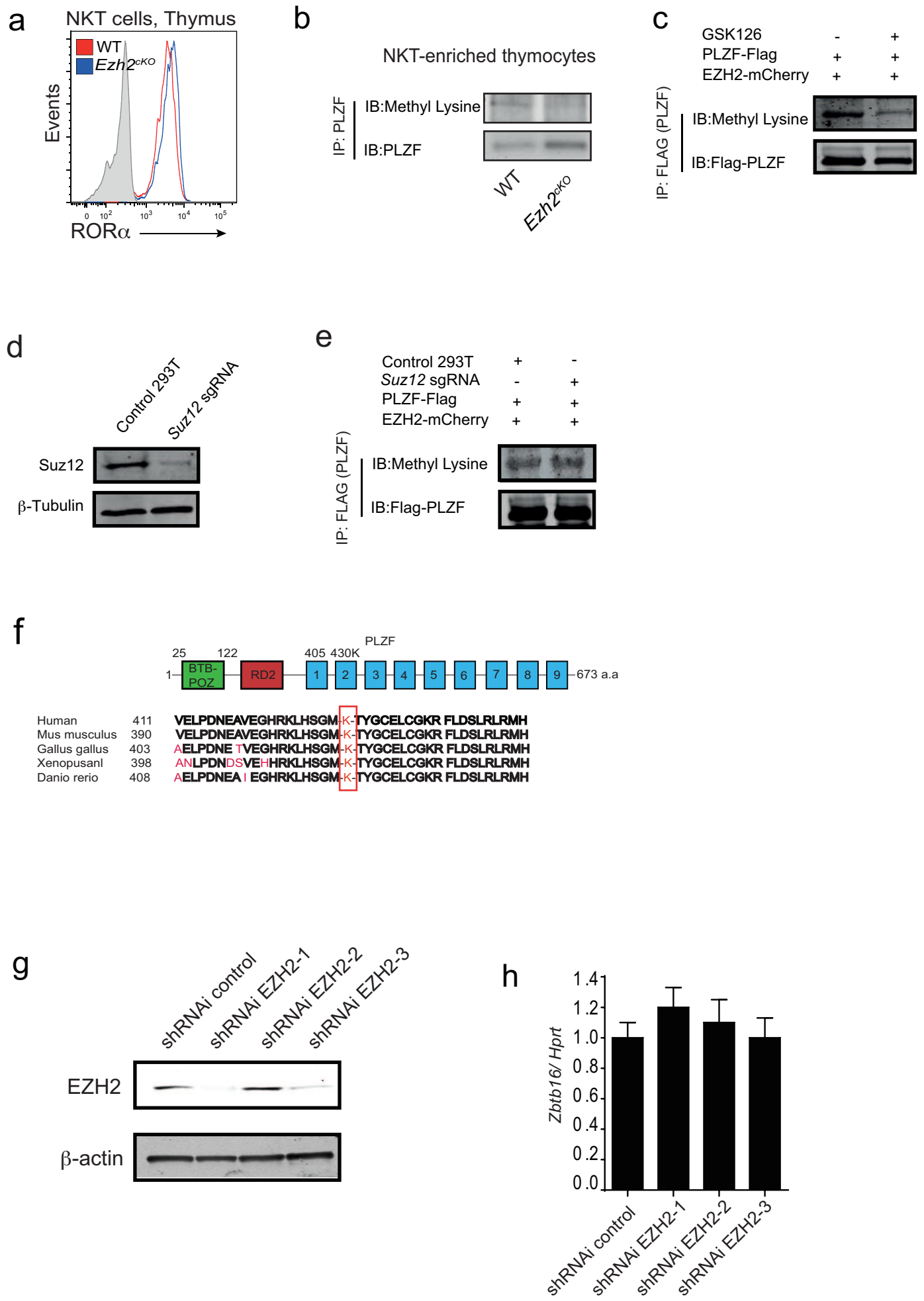
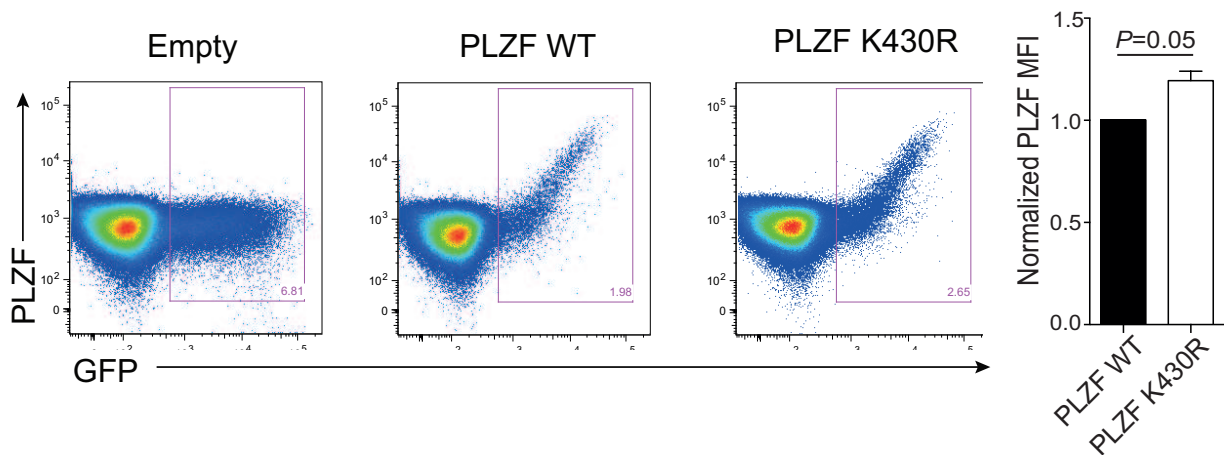
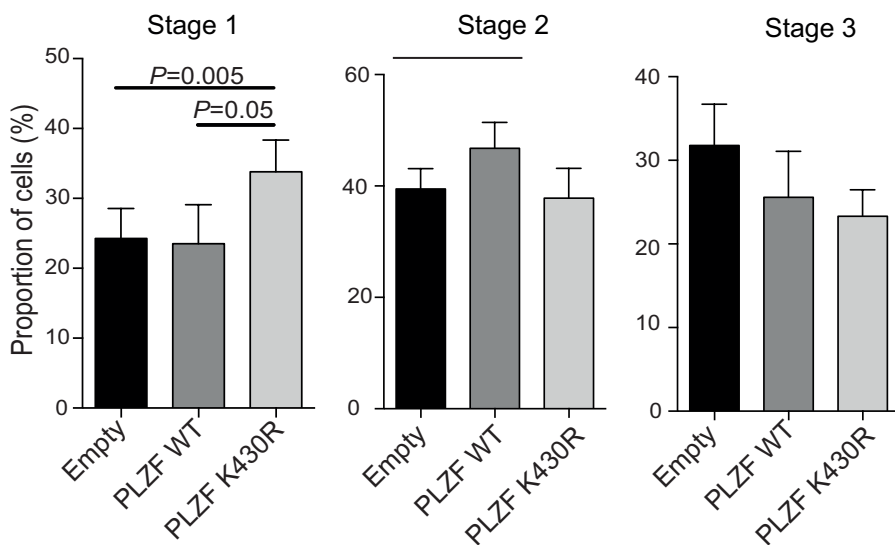


Figure EV5

a



b



c

